Final version published as: "In situ X-ray Absorption Spectroscopic Studies of Magnetic Fe@FexOy/Pd Nanoparticle Catalysts for Hydrogenation Reactions," Yao, Y.; Rubino, S.; Gates, B.D.; Scott, R.W.J.; Hu, Y., Catalysis Today, 2017, 291, 180-186. DOI: 10.1016/j.cattod.2017.02.049.

Understanding the Activity and Stability of Magnetic $Fe@Fe_xO_y/Pd$ Nanoparticle Catalysts

Yali Yao[1], Stefano Rubino,[2] Byron D. Gates,[2] Yongfeng Hu[3]*, Robert W. J. Scott[1]*

[1] Department of Chemistry, University of Saskatchewan, 110 Science Place, Saskatoon, SK, S7N 5C9, Canada

[2] Department of Chemistry and 4D LABS, Simon Fraser University, Burnaby, BC, V5A 1S6, Canada

[3]Canadian Light Source, University of Saskatchewan, Saskatoon, SK S7N 2V3, Canada

*Corresponding authors

E-mail: yongfeng.hu@lightsource.ca, voice: 306-657-3722

E-mail: robert.scott@usask.ca, voice: 306-966-2017

ABSTRACT

Core@shell Fe@Fe_xO_y nanoparticles (NPs) have attracted a great deal of interest as potential magnetic supports for catalytic metals via galvanic exchange reactions. In this study Fe@Fe_xO_y/Pd bimetallic NPs were synthesized through galvanic exchange reactions using 50:1, 20:1 and 5:1 molar ratios of Fe@Fe_xO_y NPs to $Pd(NO_3)_2$. The resulting Fe@Fe_xO_y/Pd NPs have Pd nanoparticles on the Fe oxide surfaces, and the NPs are linked in chains as shown by TEM analysis and EDX mapping. After galvanic reactions with Pd, the particles still retain their response to external magnetic fields. The magnetic properties of the resulting materials led to their successful application as nanometer-sized magnetic stir bars for hydrogenation reactions. The Fe@Fe_xO_y/Pd NPs derived from the 5:1 molar ratio of their respective salts (Fe:Pd) exhibited a higher catalytic activity than particles synthesized from 20:1 and 50:1 molar ratios for the hydrogenation of 2-methyl-3-buten-2-ol. The highest turnover frequency reached 3600 h^{-1} using ethanol as a solvent. *In situ* X-ray absorption near edge structure (XANES) spectra show that the Fe@Fe_xO_y core shell particles in the Fe@Fe_xO_y/Pd system are easily oxidized when dispersed in water, while they are very stable if ethanol is used as a solvent. This oxidative stability has important implications for the use of such particles in real world applications.

KEYWORDS: Fe@Fe_xO_y/Pd nanoparticles, nanometer-sized magnetic stir bar, *in situ* XANES study, hydrogenation reactions

INTRODUCTION

Nanoparticles (NPs) can have dramatically different properties compared to their bulk counterparts due to their large surface-to-volume ratios and size-dependent electronic properties.[1,2] They have broad applications in catalysis, drug delivery, environmental remediation.[3-6] Because of their small sizes, the separation of NPs from solutions after applications can be particularly problematic. Magnetic Fe or Fe oxide NPs have attracted tremendous attention, because they can be isolated from the liquid medium by simply applying an external magnetic field.[7-9] Moreover, Fe or Fe oxide NPs can respond to common magnetic stirrers, which opens up the possibilities of using them as nanoscale magnetic stir bars for mass transfer acceleration in microfluidic systems. For example, Chen's group assembled Fe_3O_4 NPs to form 1D chains preserved in a shell of silica.[10] The resulting Fe_3O_4 chains remain suspended and stir independently within a small liquid droplet. Song's group grafted Pd NPs on the surfaces of Fe_3O_4 nanochains using poly(cryclotriphosphazene-*co*-4,4'-sulfonyldiphenol (PZS), and applied these nanochains as catalysts and nanometer-sized magnetic stir bars for microscopic hydrogenation reactions.[11] Considering that metallic Fe NPs also have interesting magnetic behavior, further studies into their magnetic performance and stability are required for applications in catalysis and microfluidic research.

Both Fe(0) and Fe(II) have relatively low standard electrode potentials (Fe^{2+}/Fe^0, $E^o_{½}$ = -0.447 V, Fe^{3+}/Fe^{2+}, $E^o_{½}$ = 0.771 V), so they can be used to reduce another metal onto their surfaces to form bimetallic NPs through galvanic exchange reactions.[12] Many

bimetallic NPs, such as FePd, FeCu, FeRu, have been synthesized successfully by this method.[13-16] Recently, we showed that Fe@Fe_xO_y NPs are very effective reductants for galvanic exchange reactions which can fully reduce Pd or Cu salts onto their surfaces to form Pd or Cu NPs.[17] We also demonstrated that these galvanic reactions can be monitored by *in situ* X-ray absorption spectroscopy (XAS). Depending on the metal deposited on the Fe@Fe_xO_y NPs, the resulting bimetallic NPs can be used to further catalyze a variety of organic reactions. For example, Moores' group has shown that Fe@Fe_xO_y@Cu NPs are active for the heterogeneous azide-alkyne click reactions and the cyclopropanation of diazoesters with styrene derivatives,[14,18] and Zhou and coworkers have reported that Fe@Fe_xO_y@Pd NPs are active catalysts for Suzuki-Miyaura cross-coupling reactions.[13] Pd can catalyze not only C-C coupling reactions, but also a myriad of hydrogenation reactions, and Pd/C is widely used as a catalyst for hydrogenation reactions.[19-21] A variety of supports have also been investigated to further improve the catalytic activity, stability and selectivity of Pd sites in different hydrogenation reactions. He and coworkers reported that covalent trizaine (CTF) framework-supported Pd NPs exhibit *ca*. 3.6 times faster reaction rates than Pd/C for the catalytic hydrogenation of N-methylpyrrole; the accelerated rate was attributed to intensified electronic interactions between the Pd NPs and the CTF.[22] The Fe_3O_4-PZS-Pd nanochains show much better stability during cycling tests for the hydrogenation of styrene in comparison with commercial Pd/C, because the interaction between PZS and Pd can efficiently prevent the aggregation of Pd NPs and the magnetic Fe_3O_4 component can assist with recovering these nanomaterials with almost no loss.[11] Studies of Fe-

supported Pd NPs for catalytic hydrogenations are rare.[23] For many applications of the bimetallic NPs based on Fe as mentioned above, it is of great interest to investigate the performance of $Fe@Fe_xO_y@Pd$ NPs for hydrogenation reactions.

The study of the nature of a catalyst and the identity of its active site is important to improve its performance in catalytic reactions. *In situ* and *operando* characterizations of catalysts have been widely practiced by researchers, because they can directly probe catalysts under working conditions. Among various *in situ* techniques, X-ray absorption near edge structure (XANES) spectra are sensitive to the oxidation state and coordination environment of an element and can be used to probe short-range order within materials, and thus it is a useful technique for the characterization of metal NPs in solution.[24-27] We have previously shown that both Fe metal oxidation and galvanic redox reactions of $Fe@Fe_xO_y$ particles with Pd(II) and Cu(II) can be followed by *in situ* XANES.[17,28] Coordination environment changes can also be followed; for example, recently we monitored the reaction of Pd(II) acetate with $Au_{25}(SC_8H_9)_{18}^-$ clusters, and found that Pd(II) acetate was converted to Pd(II) thiolate species through the reaction with S atoms in the staple motifs (-S-Au-S-Au-S-) of the $Au_{25}(SC_8H_9)_{18}^-$ clusters as determined from the changes in the XANES spectra.[29] Based on the results of *in situ* Au L_3-edge XANES spectra on supported-partially oxidized Au NPs, Haider *et al*. proposed that metallic Au is the active species in the aerobic liquid-phase oxidation of alcohol oxidation. The conversion of 1-phenylethanol in the oxidation reaction increased with the concomitant reduction of Au species and did not decrease even after the disappearance of oxidized Au species.[30]

Herein, we have synthesized Fe@Fe_xO_y/Pd NPs with different molar ratios of Fe to Pd (50:1, 20:1 and 5:1) through galvanic exchange reactions. We also applied the 50:1 and 20:1 Fe@Fe_xO_y/Pd NPs as nanometer-sized magnetic/catalytic stir bars for the hydrogenation of 2-methyl-3-buten-2-ol separately in a solution of either water or ethanol. Additionally, we carried out *in situ* XANES experiments to study catalytic speciation in different solvents during the hydrogenation reaction, to better understand differences in catalytic behavior in the different solvents. The magnetic response of 50:1 and 20:1 Fe@Fe_xO_y/Pd NPs shows that they hold promise for the design of real nanometer-sized magnetic stir bars for microscopic reactions. The results of the studies indicated that Fe@Fe_xO_y/Pd NPs have a higher catalytic activity in ethanol compared to water for hydrogenation reactions, and *in situ* XANES experiments reveal that these NPs are more stable in ethanol solution, whereas further oxidation of the Fe cores occurs in the present of water.

EXPERIMENTAL SECTION

Materials. All chemicals were used as received without further purification. Iron (II) sulfate heptahydrate and methylene blue were purchased from Sigma-Aldrich. Poly(vinylpyrrolidone) (M. W. 58,000 g/mol), 2-methyl-3-buten-2-ol, 2-methylbutan-2-ol and palladium (II) nitrate hydrate were purchased from Alfa Aesar. Sodium borohydride, ethanol and methanol (HPLC grade) were purchased from Fisher Scientific. Sulfuric acid was purchased from EMD Millipore. Eighteen MΩ·cm Milli-Q water (Millipore, Bedford, MA) was used for all syntheses.

Synthesis of Fe@Fe_xO_y/Pd NPs. Fe@Fe_xO_y NPs were synthesized by reducing $FeSO_4 \cdot 7H_2O$ (5.0 mmol) by $NaBH_4$ (25 mmol) in a 1:1 water/methanol (v/v) mixture (20 mL) in the presence of PVP (10 mmol based on monomer unit) under nitrogen gas as previously reported.[28] Then 5.0 mL of 1 M H_2SO_4 was added to remove any excess $NaBH_4$ before injecting a Pd(II) nitrate solution (20 mM) to react with the Fe@Fe_xO_y NPs by galvanic exchange reactions.

Hydrogenation of Methylene Blue. A solution of $NaBH_4$ with Fe@Fe_xO_y/Pd NPs was prepared by dispersing 0.50 mL of the above solution of Fe@Fe_xO_y/Pd NPs and 0.038g sodium borohydride in 10 mL water. A 25 μL aliquot of this mixture was injected into a 25 μL methylene blue solution (0.050 mM), which was dropped onto a hydrophobic Teflon plate located on top of a magnetic stirrer.

Hydrogenation of 2-methyl-3-buten-2-ol. A solution of 0.010 mmol Fe@Fe_xO_y/Pd NPs (molar concentration determined based on Pd content) in 5.0 mL water was added to a round bottom flask filled with 1.1 atm hydrogen gas. To this solution, a 0.20 mL 2-methyl-3-buten-2-ol (1.9 mmol) solution was added to obtain a 190:1 substrate to catalyst molar ratio. The pressure was monitored by a differential pressure manometer (407910, Extech Instrument), and the reaction progress was also followed by ^1H NMR by extracting products from the reaction solutions with 2 mL aliquots of $CDCl_3$. Turnover frequencies (TOFs) were measured by plotting either product conversion or H_2 consumption (as a proxy for product conversion, a direct correspondence between NMR results and H_2 pressure decay was always observed) over reaction time. These results are reported in either (mols product formed/ moles Pd)/time or (moles H_2

consumed/mole Pd)/time.

Characterization. Transmission electron microscopy (TEM) analyses of the NPs were initially conducted using a HT7700 microscope (Hitachi High-Technologies) operating at 100 kV. The samples were prepared by drop-casting one drop of dilute, aqueous sample onto a carbon-coated 200 mesh copper grid (Electron Microscopy Sciences, Hatfield, PA).

Elemental maps were obtained using an FEI Osiris STEM equipped with ChemiSTEM Technology integrating the signal from four Energy Dispersive X-ray (EDX) spectrometers. A 200 kV electron beam was focused to a nanometer-sized spot and scanned across the sample to excite electrons from the core shells. As the electron beam is raster scanned across the sample, a full X-ray spectrum is collected for each pixel. By selecting the appropriate energy window, a specific element is selected and its distribution in the sample can be displayed as an elemental map. By selecting several windows, different elemental maps can be obtained simultaneously from a single scan, provided that the ionization energies do not significantly overlap. False color maps can be also superimposed to determine where two or more elements coexist and in what relative amounts. Scanning time and beam intensity were chosen as a compromise between signal-to-noise ratio and radiation damage to the sample.

Fe K-edge and Pd L-edge XANES spectra were collected at the Soft X-ray Microcharacterization Beamline (SXRMB) at the Canadian Light Source (CLS). The measurements were conducted under an ambient atmosphere for observing the Fe K-edge and under helium for obtaining the Pd L_3-edge spectra. Decreasing the beam flux

by defocusing and/or filtering the beam with Kapton filters and stirring the sample via magnetic stirring were used to avoid sample damage due to photoreduction. Liquid cells (SPEX CertiPrep Disposable XRF X-Cell sample cups) were covered with a 4 μm ultralene film (purchased from Fisher Scientific, Ottawa, ON) and used for XANES analysis. The data were analyzed using the IFEFFIT software package.[31,32]

The ^{1}H NMR spectra were recorded in $CDCl_3$ on a Bruker 500 MHz Advance NMR spectrometer. Chemical shifts were recorded in parts per million (ppm), using the residual solvent peak for calibration. The composition of the reaction mixture was analyzed by a gas chromatography (GC, Agilent Technologies 7890A) with a flame ionization detector and a HP-5 capillary column (30 m × 0.32 mm × 0.25 μm, J&W Scientific).

RESULTS AND DISCUSSION

Synthesis and STEM Analysis of Fe@Fe_xO_y/Pd NPs. The Fe@Fe_xO_y NPs (16.0 ± 6.0 nm) were synthesized by reducing $FeSO_4 \cdot 7H_2O$ with $NaBH_4$ in a mixture of ethanol and water (1:1 volume ratio) containing PVP as a stabilizer.[28] Different molar ratios of Fe@Fe_xO_y/Pd (prepared as 50:1, 20:1, and 5:1 based on Fe:Pd molar ratios) NPs were synthesized by mixing the solution of Fe@Fe_xO_y NPs with a Pd(II) nitrate solution under nitrogen gas purging as described previously.[17] Figure 1A and 1C show dark field STEM images of the particles synthesized at the 20:1 and 5:1 Fe:Pd molar ratios. As seen previously, the Fe@Fe_xO_y particles self-assemble into larger nanostructures. As shown in the STEM elemental maps (Figure 1B and 1D), the 20:1 Fe@Fe_xO_y/Pd NPs

have isolated small Pd NPs (3 ± 2 nm) deposited on the surfaces of the Fe@Fe_xO_y NPs. In the system of 5:1 Fe@Fe_xO_y/Pd NPs most of the Fe@Fe_xO_y NPs have been consumed in the galvanic exchange formation, leaving a hybrid material that contains a fairly well-dispersed Pd on the surfaces of these Fe oxide supports. It was very difficult to resolve individual Pd NPs in the samples containing a higher Pd loading.

Fe@Fe_xO_y/Pd NPs as Nanometer-sized Magnetic Stir Bars. Fe supported bimetallic NPs have been applied in a variety of catalytic reactions.[13-16,33,34] The presence of Fe in these bimetallic NPs not only allows them to be easily separated from reaction solutions by an external magnet, but can also act as a redox scavenger to redeposit the leached metal and avoid the contamination of the organic product. Fe atoms have a strong magnetic moment due to their high number of unpaired 3d electrons, thus Fe and Fe oxide materials exhibit strong magnetic properties.[35] The large surface area to volume ratio of Fe and Fe oxide NPs can result in increased remanence and coercivity and can give these NPs improved magnetic properties in comparison to their bulk counterparts.[36,37] The fact that the original Fe@Fe_xO_y NPs self-assemble into larger domains may allow them to be used for stirring at the microscopic scale. Indeed this is the case for the Fe@Fe_xO_y/Pd NPs synthesized with 50:1 and 20:1 molar ratios of Fe@Fe_xO_y NPs to Pd(II). The resulting NPs have strong responses to the magnetic field of a common stir plate, and allow for a solution to be stirred in the absence of a macroscopic stir bar (Figure S1). However, the Fe@Fe_xO_y/Pd NPs synthesized with a 5:1 molar ratio of Fe@Fe_xO_y NPs to Pd(II) do not agitate a solution upon magnetic stirring. In addition, we examined the relative ease of magnetically separating each of

the NP systems from solution. The 50:1 and 20:1 Fe@Fe_xO_y/Pd NPs could be separated by an external magnet from the reaction solutions after 9 s (Figure S2), while the separation of the 5:1 Fe@Fe_xO_y/Pd NPs from solution takes a much longer time (more than 30 s). These results indicate the possibility of using these bimetallic catalysts as microscopic stir bars and magnetically recoverable catalysts, provided that the Pd loading is not too high.

To further test the ability of the Fe@Fe_xO_y/Pd NPs act as microscopic stir bars in solution, a model test system was carried out using the hydrogenation of methylene blue (MB) within small liquid droplets. Solutions containing either 50:1 or 20:1 Fe@Fe_xO_y/Pd NPs and $NaBH_4$ were injected into the MB droplet. MB could be reduced by the $NaBH_4$ and converted to a colorless leucomethylene blue solution in 30 seconds when agitated by the 50:1 or 20:1 Fe@Fe_xO_y/Pd NPs (Figure S3). In comparison, it was difficult to reduce MB by the addition of $NaBH_4$ without the stirring of NPs. This study reveals that the agitation of the 50:1 and 20:1 Fe@Fe_xO_y/Pd NPs using an external magnetic field can effectively mix the reactants and improve the reaction rate. We also tested the Fe@Fe_xO_y/Pd NPs as catalysts and microscopic stirrers for the hydrogenation of 2-methyl-3-buten-2-ol in water under a 1.1 atm H_2 gas (Scheme 1). The progress of the reaction was monitored by measuring the decrease in pressure of H_2 filled in a round bottom flask as a function of reaction time, and the final product was characterized by ^{1}H NMR. When only Fe@Fe_xO_y NPs were used as the catalysts for this reaction, there was no decrease in the pressure of H_2. However, the addition of the 50:1 Fe@Fe_xO_y/Pd NPs as catalysts yielded a TOF of 21 h^{-1} for the hydrogenation of 2-methyl-3-buten-2-

ol to 2-methyl-2-butanol as determined by NMR in the absence of stirring, whereas the TOF was improved to 34 h^{-1} by stirring the solution using the 50:1 Fe@Fe_xO_y/Pd NPs (Figure 2). This result shows that Pd is the active catalyst, and confirms that the NPs can improve mass-transfer of the substrates to the catalyst surface. As this test was performed on a 5mL sample and not a droplet with a small volume, the difference between the stirred and non-stirred states is not as significant as noted earlier for the reduction of MB. The ability of the NPs to effectively stir larger volumes of solutions is significantly lower in comparison to the use of macroscopic stir bars. In addition, while the NPs can agitate solutions and thus ensure good mixing in single phase systems, resolving mass transfer effects relating to hydrogen gas dissolution into solution requires a significant agitation such that the surface area of the solution/gas interface is increased. This agitation is not possible using the NPs as microscopic stir bars within the proportionally large volume of solution.

Catalytic Behavior in the Hydrogenation of 2-methyl-3-buten-2-ol. Having established that the Fe@Fe_xO_y/Pd NPs can be effectively catalyze reactions in solution, we sought to optimize the catalyst system in terms of the Pd loading, solvent composition, and long-term stability of the catalyst. For these studies larger volumes of solutions were used along with a macroscopic magnetic stir bar (egg shaped, 7/8 inch × 3/8 inch) rotated at 1600 rpm to minimize mass transfer effects for the hydrogenation reactions and thus better compare actual catalytic activities. The Fe@Fe_xO_y/Pd NPs (50:1, 20:1 and 5:1 Fe:Pd molar ratios) each catalyzed the hydrogenation of 2-methyl-3-buten-2-ol in water at 1.1 atm H_2 (g) and 25 °C, as shown in Figure 3. The results

indicate that the reaction follows a zero order rate law, and reaches completion once all the substrate is consumed. The decrease of the moles of the H_2 gas in the reaction from 0.0482 mol to 0.0463 mol reveals that the consumption of H_2 is 1:1 with respect to the substrate 2-methyl-3-buten-2-ol (1.9 mmol used for the reaction). The 5:1 Fe@Fe_xO_y/Pd NPs showed the highest TOF (*ca.* 1300 h^{-1}) in comparison to the 50:1 and 20:1 Fe@Fe_xO_y/Pd NPs (TOF of 385 h^{-1} and 785 h^{-1}, respectively). As noted earlier, Fe@Fe_xO_y NP controls showed no activity for hydrogenations, confirming that Pd is the active catalyst for this reaction. The higher TOF of 5:1 Fe@Fe_xO_y/Pd NPs compared to 50:1 and 20:1 Fe@Fe_xO_y/Pd NPs suggests that the Pd is more dispersed and has a higher surface area for the 5:1 Fe@Fe_xO_y/Pd NPs, which is in agreement with the results of elemental EDX maps shown earlier.

The reusability of the Fe@Fe_xO_y/Pd NPs was also examined by using 20:1 Fe@Fe_xO_y/Pd NPs as an example. These NPs were recycled by isolating the NPs from solution using centrifugation. The results of this evaluation are summarized in Figure 4. Surprisingly, the Fe@Fe_xO_y/Pd NPs exhibited a higher catalytic activity upon recycling. However, it also became successively more difficult to fully recover the material with an external magnet. The TEM images show that there are fewer and/or significantly smaller Fe@Fe_xO_y NPs remaining in the bimetallic NPs system as the number of cycles increased (Figure 5). The result suggests that the Fe@Fe_xO_y NPs are degrading over time. This conclusion is also supported by *ex situ* X-ray absorption near-edge structure (XANES) spectroscopy measurements, as shown in Figure 6. There is almost no change in the speciation of the zerovalent Pd NPs as judged by comparing

the Pd L_3-edge XANES spectra after different recycling tests (Figure 6A), while the Fe K-edge XANES spectra show a significant shift to higher energies upon using the catalysts over 6 cycles (Figure 6B). These results are consistent with the progressive oxidation of the Fe@Fe_xO_y NPs to Fe(II) and Fe(III) oxides.[28]

To determine whether the oxidation of Fe@Fe_xO_y NPs takes place during the hydrogenation reaction or during the recycling process, *in situ* XANES studies were carried out. The *in situ* setup is shown in Figure 7, and consisted of a liquid cell loaded with Fe@Fe_xO_y NPs and 2-methyl-3-buten-2-ol in water, and placed inside an aluminum box which was located on top of a magnetic stirrer (not shown) to ensure the constant mixing of the reaction mixture. Hydrogen gas was bubbled into the liquid cell to start the reaction and the reaction was monitored at the Pd L_3 and Fe K edges, as shown in Figure 8. No significant change of the *in situ* Pd L_3-edge XANES spectra was observed (Figure 8A), which is not overly surprising as Pd typically remains in the zerovalent state during hydrogenation reactions.[38] However, slight oxidation of the Fe@Fe_xO_y NPs could be observed from *in situ* Fe K-edge XANES spectra (Figure 8B). Through fitting the Fe K-edge XANES spectra using a linear combination fitting with standards (Fe foil, $FeSO_4$ and $Fe(NO_3)_3$), it is revealed that the Fe@Fe_xO_y NPs in the Fe@Fe_xO_y/Pd NP systems contain 56% Fe(0) (Table S1). This Fe(0) content decreases to 49% after 30 min of the hydrogenation reaction in water, and all the Fe(0) was oxidized after 6 cycles (to 60% Fe(II) and 40% Fe(III), the fitted data from Figure 6B, Table S2). This result indicates that the oxidation of Fe@Fe_xO_y NPs happens during the reaction. We note that water as the solvent for this reaction; water can react with

exposed Fe in Fe@Fe_xO_y NPs and oxidize Fe(0) to Fe(II), which is likely the reason for oxidation of the Fe@Fe_xO_y NPs in the reaction.[39] The Fe(II) is then further oxidized to Fe(III) during the recycling process when the samples are exposed to air.

In order to address this oxidation damage to the NPs, we switched the solvent from water to ethanol for the hydrogenation reactions, as ethanol should not react with Fe(0). The Pd L_3-edge XANES spectra indicate that the Pd NPs have no change before and after the hydrogenation reaction in ethanol (Figure S4). There is also no change observed in the *in situ* Fe K-edge XANES spectra (Figure 9). These results confirm that the Fe@Fe_xO_y NPs are quite stable in ethanol. The Fe@Fe_xO_y/Pd NPs also showed a much higher catalytic activity in ethanol than in water, as shown in Figure 10. The 5:1 Fe@Fe_xO_y/Pd NPs showed improvements in TOF from *ca*. 1300 h^{-1} in water to 3600 h^{-1} in ethanol, an increase of 2.8 times in magnitude. The NMR and GC results confirmed that the conversion of 2-methyl-3-buten-2-ol to 2-methylbutan-2-ol is completed in 4 min when catalyzed by 5:1 Fe@Fe_xO_y/Pd NPs with a 190:1 substrate to catalyst ratio in ethanol. This catalytic result is a very high TOF for the hydrogenation of 2-methyl-3-buten-2-ol under ambient conditions, and compares favourably with many excellent hydrogenation catalysts in the literature.[40-43] The factors determining solvent influence in the hydrogenation reactions have been studied by many groups.[38,44-48] The solubility of H_2 (g) seems to be the most significant factor influencing the rate of this reaction along with the high stability of the support in ethanol. The solubility of H_2 (2.98×10^{-3} mol/L) in ethanol is significantly higher than that in water (0.81×10^{-3} mol/L).[49] These results are also consistent with Nikoshvili group's studies

on the selective and solvent dependent hydrogenation of 2-methyl-3-butyn-2-ol to 2-methyl-3-buten-2-ol over Pd NPs stabilized in hypercrosslinked polystyrene.[38]

CONCLUSION

A suspension of either 50:1 or 20:1 Fe@Fe_xO_y/Pd NPs can act as both catalysts and microscopic magnetic stir bars to improve the mixing of reactants and help prevent mass transfer issues in catalytic hydrogenation reactions. For studies on the catalytic activity of the Fe@Fe_xO_y/Pd NPs for the hydrogenation of 2-methyl-3-buten-2-ol, the 5:1 molar ratio Fe@Fe_xO_y/Pd NPs exhibit a high TOF of 3600 h^{-1} using ethanol as the solvent. *In situ* XANES spectra show that water as a solvent in the hydrogenation reaction can oxidize the Fe(0) core in Fe@Fe_xO_y/Pd NPs, while the same Fe@Fe_xO_y/Pd NPs are very stable when dispersed in ethanol. This result shows that while these composite materials have viability as low cost, magnetically recoverable catalysts, they do not have long-term stability in water which may limit their possible applications.

ACKNOWLEDGEMENTS

The authors acknowledge financial assistance from the National Sciences and Engineering Research Council of Canada (NSERC) and the Canada Research Chairs Program (B. D. Gates). XANES experiments described in this paper were performed at the Canadian Light Source, which is supported by NSERC, the National Research Council Canada, the Canadian Institutes of Health Research, the Province of Saskatchewan, Western Economic Diversification Canada, and the University of

Saskatchewan. This work also made use of 4D LABS (www.4dlabs.ca) shared facilities supported by the Canada Foundation for Innovation (CFI), British Columbia Knowledge Development Fund (BCKDF), Western Economic Diversification Canada, and Simon Fraser University.

REFERENCES

(1) Haruta, M.; Kobayashi, T.; Sano, H.; Yamada, N. Novel gold catalysis for the oxidation of carbon monoxide at a temperature far below 0 °C. *Chem. Lett.* **1987**, *2*, 405–408.

(2) Jagadeesh, R. V.; Surkus, A.; Junge, H.; Pohl, M.; Radnik, J.; Huan, H.; Schünemann, V.; Brückner, A.; Beller, M. Nanoscale Fe_2O_3-based catalysts for selective hydrogenation of nitroarenes to anilines. *Science* **2013**, *342*, 1073–1076.

(3) Zhang, H.; Jin, M.; Xia, Y. Enhancing the catalytic and electrocatalytic properties of Pt-based catalysts by forming bimetallic nanocrystals with Pd. *Chem. Soc. Rev*. **2012**, *41*, 8035–8049.

(4) Sun, T.; Zhang, Y. S.; Pang, B.; Hyun, D. C.; Yang, M.; Xia, Y. Engineered nanoparticles for drug delivery in cancer therapy. *Angew. Chem. Int. Ed*. **2014**, *53*, 12320-12364.

(5) Kaur, A.; Gupta, U. A review on applications of nanoparticles for the preconcentration of environmental pollutants. *J. Mater. Chem.* **2009**, *19*, 8279-8289.

(6) Sachan, R.; Malasi, A.; Ge, J.; Yadavali, S.; Krishna, H.; Gangopadhyay, A.; Garcia, H.; Duscher, G.; Kalyanaraman, R. Ferroplasmons: intense localized surface plasmons in metal-ferromagnetic nanoparticles. *ACS Nano* **2014**, *8*, 9790–9798.

(7) Schejn, A.; Mazet, T.; Falk, V.; Balan, L.; Aranda, L.; Medjahdi, G.; Schneider, R. Fe_3O_4@ZIF-8: magnetically recoverable catalysts by loading Fe_3O_4 nanoparticles inside a zinc imidazolate framework. *Dalton Trans*. **2015**, *44*, 10136–10140.

(8) Hudson, R.; Feng, Y.; Varma, R. S.; Moores, A. Bare magnetic nanoparticles: sustainable synthesis and applications in catalytic organic transformations. *Green Chem*. **2014**, *16*, 4493–4505.

(9) Li, A. Y.; Kaushik, M.; Li, C.-J.; Moores, A. Microwave-assisted synthesis of magnetic carboxymethyl cellulose-embedded Ag-Fe_3O_4 nanocatalysts for selective carbonyl hydrogenation. *ACS Sustainable Chem. Eng*. **2016**, *4*, 965–973.

(10) Chong, W. H.; Chin, L. K.; Tan, R. L. S.; Wang, H.; Liu, A. Q.; Chen, H. Stirring in suspension: nanometer-sized magnetic stir bars. *Angew. Chem. Int. Ed*. **2013**, *52*, 8570-8573.

(11) Yang, S.; Cao, C.; Sun, Y.; Huang, P.; Wei, F.; Song, W. Nanoscale magnetic stirring bars for heterogeneous catalysis in microscopic systems. *Angew. Chem. Int. Ed*. **2015**, *54*, 2661-2664.

(12) *CRC Handbook of Chemistry and Physics*, 96th ed.; CRC Press: Cleveland, OH, **2010**.

(13) Zhou, S.; Johnson, M.; Veinot, J. G. C. Iron/iron oxide nanoparticles: a versatile support for catalytic metals and their application in Suzuki-Miyaura cross-coupling reactions. *Chem. Commun*. **2010**, *46*, 2411–2413.

(14) Hudson, R.; Li, C.-J.; Moores, A. Magnetic copper-iron nanoparticles as simple teterogeneous catalysts for the azide-alkyne click reaction in water. *Green Chem*. **2012**, *14*, 622–624.

(15) Hudson, R.; Chazelle, V.; Bateman, M.; Roy, R.; Li, C.-J.; Moores, A. Sustainable synthesis of magnetic ruthenium-coated iron nanoparticles and application in the catalytic transfer hydrogenation of ketones. *ACS Sustain. Chem. Eng*. **2015**, *3*, 814–820.

(16) Zhang, Y.; Su, Y.; Zhou, X.; Dai, C.; Keller, A. A. A new insight on the core-shell structure of zerovalent iron nanoparticles and its application for Pb(II) sequestration. *J. Hazard. Mater.* **2013**, *263*, 685–693.

(17) Yao, Y.; Patzig, C.; Hu, Y.; Scott, R. W. J. In situ X-ray absorption spectroscopic study of Fe@Fe_xO_y/Pd and Fe@Fe_xO_y/Cu nanoparticle catalysts prepared by galvanic exchange reactions. *J. Phys. Chem. C* **2015**, *119*, 21209-21218.

(18) Ishikawa, S.; Hudson, R.; Masnadi, M.; Bateman, M.; Castonguay, A.; Moores, A.; Li, C. –J. Cyclopropanation of diazoesters with styrene derivatives catalyzed by magnetically recoverable copper-plated iron nanoparticles. *Tetrahedron* **2014**, *70*, 6162–6168.

(19) Nishimura, S. *Handbook of Heterogeneous Catalytic Hydrogenation for Organic Synthesis*; John Wiley & Sons: New York, **2001**.

(20) Rylander, P. N. *Hydrogenation Methods*; Academic Press: New York, **1985**.

(21) Sajiki, H.; Ikaea, T.; Hirota, K. Cleavage of the THP protecting group under Pd/C-catalyzed hydrogenation conditions. *Tetrahedron Lett*. **2001**, *42*, 7699–7701.

(22) He, T.; Liu, L.; Wu, G.; Chen, P. Covalent triazine framework-supported palladium nanoparticles for catalytic hydrogenation of N-heterocycles. *J. Mater. Chem. A* **2015**, *3*, 16235-16241.

(23) Yuan, J. Preparation of 2,4-difluoroaniline by catalytic hydrogenation in the presence of Pd-Fe/TiO_2 catalyst at normal pressure. *Pesticides* **2007**, *46*, 827–829.

(24) Anderson, R. M.; Zhang, L.; Loussaert, J. A.; Frenkel, A. I.; Henkelman, G.; Crooks, R. M. An experimental and theoretical investigation of the inversion of Pd@Pt core@shell dendrimer-encapsulated nanoparticles. *ACS Nano* **2013**, *10*, 9345-9353.

(25) Wang. L.; Zhang, S.; Zhu, Y.; Patlolla, A.; Shan, J.; Yoshida, H.; Takeda, S.; Frenkel, A. I.; Tao, F. Catalysis and in situ studies of Rh_1/Co_3O_4 nanorods in reduction of NO with H_2. *ACS Catal*. **2013**, *3*, 1011-1019.

(26) Ohyama, J.; Teramura, K.; Shishido, T.; Hitomi, Y.; Kato, K.; Tanida, H.; Uruga, T.; Tanaka, T. In situ Au L_3 and L_2 edge XANES spectral analysis during growth of thiol protected gold nanoparticles for the study on particle size dependent electronic properties. *Chem. Phys. Lett*. **2011**, *507*, 105-110.

(27) Maclennan, A.; Banerjee, A.; Hu, Y.; Miller, J. T.; Scott, R. W. J. In situ X-ray absorption spectroscopic analysis of gold-palladium bimetallic nanoparticle catalysts. *ACS Catal.* **2013**, *3*, 1411-1419.

(28) Yao, Y.; Hu, Y.; Scott, R. W. J. Watching iron nanoparticles rust: an in situ X-ray absorption spectroscopic study. *J. Phys. Chem. C* **2014**, *118*, 22317-22324.

(29) Shivhare, A.; Lee, K. E.; Hu, Y.; Scott, R. W. J. Following the reactivity of $Au_{25}(SC_8H_9)_{18}^-$ clusters with Pd^{2+} and Ag^+ ions using in situ X-ray absorption spectroscopy: a tale of two metals. *J. Phys. Chem. C* **2015**, *119*, 23279-23284.

(30) Haider, P.; Grunwaldt, J. –D.; Seidel, R.; Baiker, A. Gold supported on Cu-Mg-Al and Cu-Ce mixed oxides: an in situ XANES study on the state of Au during aerobic alcohol oxidation. *J. Catal.* **2007**, *250*, 313-323.

(31) Newville, M. IFEFFIT: interactive XAFS analysis and FEFF fitting. *J. Synchrotron Radiat*. **2001**, *8*, 322-324.

(32) Ravel, B.; Newville, M. ATHENA, ARTEMIS, HEPHAESTUS: data analysis for X-ray absorption spectroscopy using IFEFFIT. *J. Synchrotron Radiat*. **2005**, *12*, 537-541.

(33) Kovács, S.; Zih-Perényi, K.; Révész, Á.; Novák, Z. Copper on iron: catalyst and scavenger for azide-alkyne cycloaddition. *Synthesis* **2012**, *44*, 3722–3730.

(34) Kovács, S.; Novák, Z. Oxidoreductive coupling of thiols with aryl halides catalyzed by copper on iron. *Org. Biomol. Chem.* **2011**, *9*, 711–716.

(35) Wasilewshi, P.; Kletetschka, G. Lodestone: natures only permanent magnet-what it is and how it gets charged. *Geophys. Res. Let.* **1999**, *26*, 2275–2278.

(36) Issa, B.; Obaidat, I. M.; Albiss, B. A. Haik, Y. Magnetic nanoparticles: surface effects and properties related to biomedicine applications. *Int. J. Mol. Sci.* **2013**, *14*, 21266-21305.

(37) Kim, D. K.; Zhang, Y.; Voit, W.; Rao, K. V.; Muhammed, M. Synthesis and characterization of surfactant-coated superparamagnetic monodispersed iron oxide nanoparticles. *J. Magn. Magn. Mater.* **2001**, *225*, 30-36.

(38) Nikoshvili, L.; Shimanskaya, E.; Bykov, A.; Yuranov, I.; Kiwi-Minsker, L.; Sulman, E. Selective hydrogenation of 2-methyl-3-butyn-2-ol over Pd-nanoparticles stabilized in hypercrosslinked polystyrene: solvent effect. *Catal.Today* **2015**, *241*, 179-188.

(39) Li, X.; Elliott, D. W.; Zhang, W. Zero-valent iron nanoparticles for abatement of environmental pollutants: materials and engineering aspects. *Crit. Rev. Env. Sci. Technol.* **2006**, *31*, 111-122.

(40) Ma. R.; Semagina, N. Nanoparticle shape effect study as an efficient tool to reveal the structure sensitivity of olefinic alcohol hydrogenation. *J. Phys. Chem. C* **2010**, *114*, 15417-15423.

(41) Shen. J.; Semagina, N. Iridium- and Platinum-Free ring opening of indan. *ACS Catal.* **2014**, *4*, 268-279.

(42) Banerjee, A.; Scott, R. W. J. Optimization of transition metal nanoparticle-phosphonium ionic liquid composite catalytic systems for deep hydrogenation and hydrodeoxygenation reactions. *Green Chem*. **2015**, *17*, 1597–1604.

(43) Niu, Y.; Yeung, L. K.; Crooks, R. M. Size-selective hydrogenation of olefins by dendrimer-encapsulated palladium nanoparticles. *J. Am. Chem. Soc*. **2001**, *123*, 6840–6846.

(44) Sadeghmoghaddam, E.; Gu, H.; Shon, Y.–S. Pd nanoparticle-catalyzed isomerization vs hydrogenation of allyl alcohol: solvent-dependent regioselectivity. *ACS Catal.* **2012**, *2*, 1838-1845.

(45) Bertero, N. M.; Trasarti, A. F.; Apesteguia, C. R.; Marchi, A. J. Catalytic and kinetic study of the liquid-phase hydrogenation of acetophenone over Cu/SiO_2 catalyst. *Appl. Catal. A: Gen.* **2011**, *394*, 228-238.

(46) Rajadhyskasha, R. A.; Karwa, S. I. Solvent effects in catalytic hydrogenation. *Chem. Eng. Sci.* **1986**, *41*, 1765-1770.

(47) Augustine, R. L.; Warner, R. W.; Melnick, M. J. Heterogeneous catalysis in organic chemistry. 3. Competitive adsorption of solvents during alkene hydrogenations. *J. Org. Chem.* **1984**, *49*, 4853-4856.

(48) Toukoniitty, E.; Mäki-Arvela, P.; Kuusisto, J.; Nieminen, V.; Päivärinta, J.; Hotokka, M.; Salmi, T.; Yu Murzin, D. Solvent effects in enantioselective hydrogenation of 1-phenyl-1,2-propanedione. *J. Mol. Catal.* **2002**, *192*, 135-151.

(49) Ghavre, M.; Morrissey, S.; Gathergood, N. in: Kokorin A. (Ed.) *Hydrogenation in Ionic Liquids, Ionic Liquids: Applications and Perspectives*. **2011**, 331-392.

Scheme 1. The hydrogenation of 2-methyl-3-buten-2-ol.

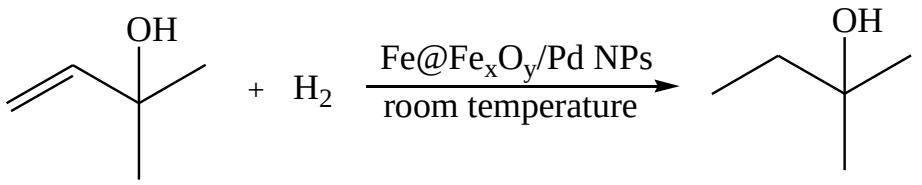

2-methyl-3-buten-2-ol (MBE) 2-methyl-2-butanol (MBA)

Figure 1. High-angle annular dark-field STEM images and EDX elemental maps of the Fe@Fe_xO_y/Pd NPs prepared from 20:1 (A and B) and 5:1 (C and D) molar ratios of Fe@Fe_xO_y NPs to Pd(II).

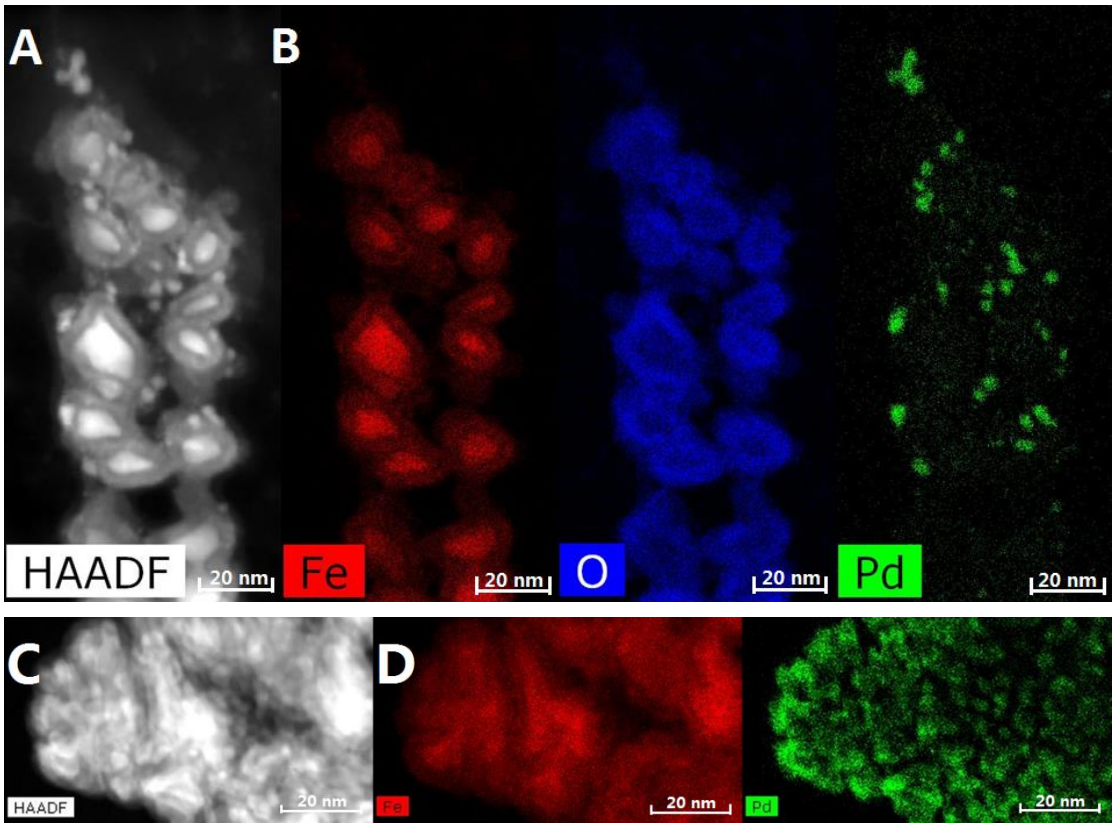

Figure 2. The conversion of 2-methyl-3-buten-2-ol to 2-methyl-2-butanol in the hydrogenation reaction (black square) using the 50:1 $Fe@Fe_xO_y/Pd$ NPs as catalysts without stirring, and (orange dot) using 50:1 $Fe@Fe_xO_y/Pd$ NPs as both catalysts and microscopic stir bars in a 5 mL solution.

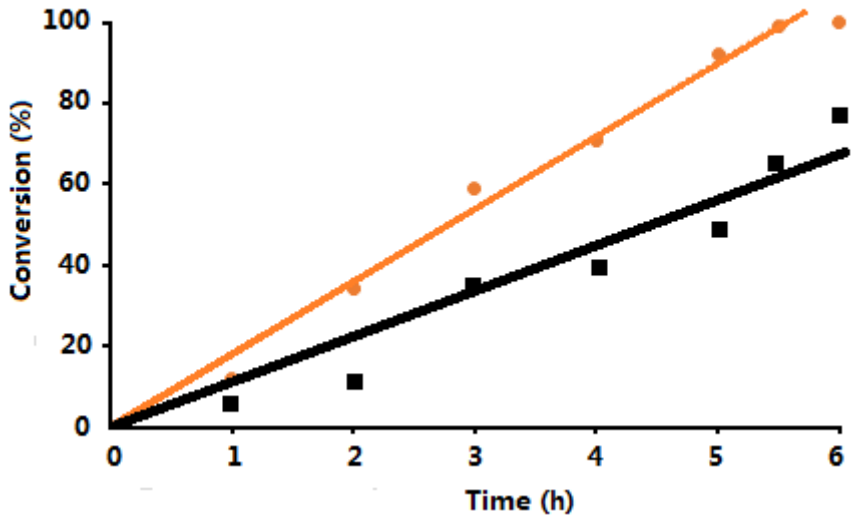

Figure 3. The rate of hydrogen consumption in the hydrogenation of 2-methyl-3-buten-2-ol in water using the 50:1 (red circle), 20:1 (blue triangle) and 5:1 (black square) Fe@Fe_xO_y/Pd NPs as catalysts.

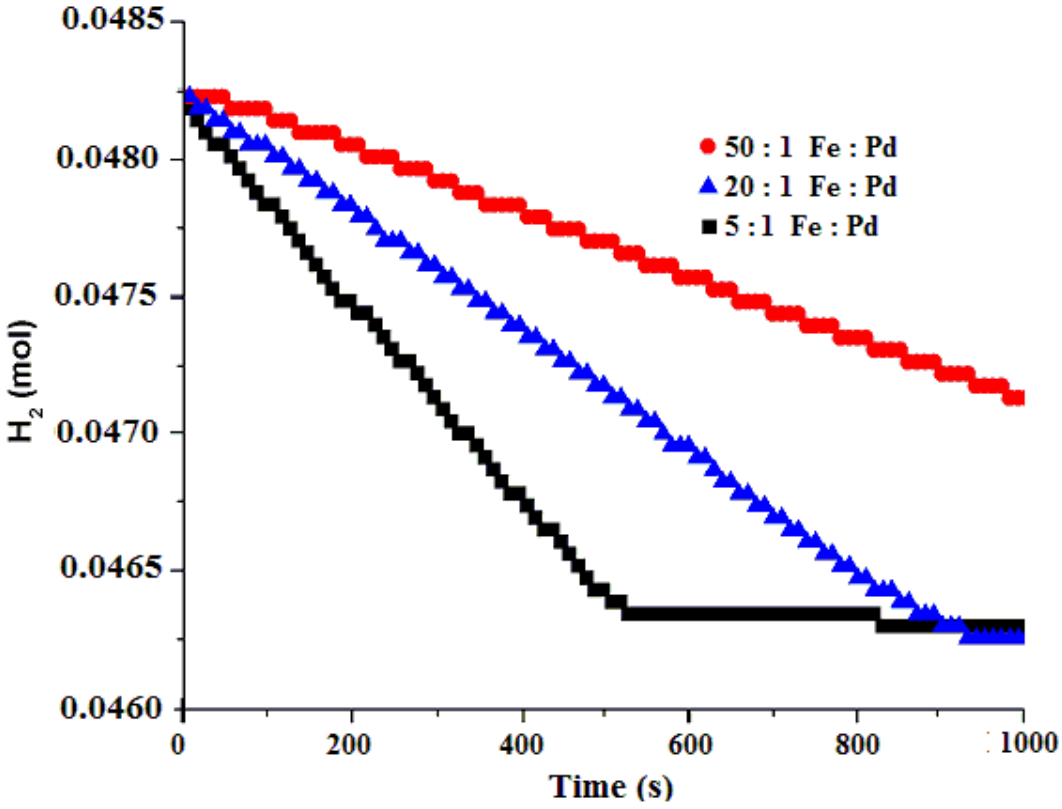

Figure 4. The rates of hydrogen consumption in the hydrogenation of 2-methyl-3-buten-2-ol in water using the 20:1 $Fe@Fe_xO_y/Pd$ NPs recycled for the use in sequential catalytic cycles.

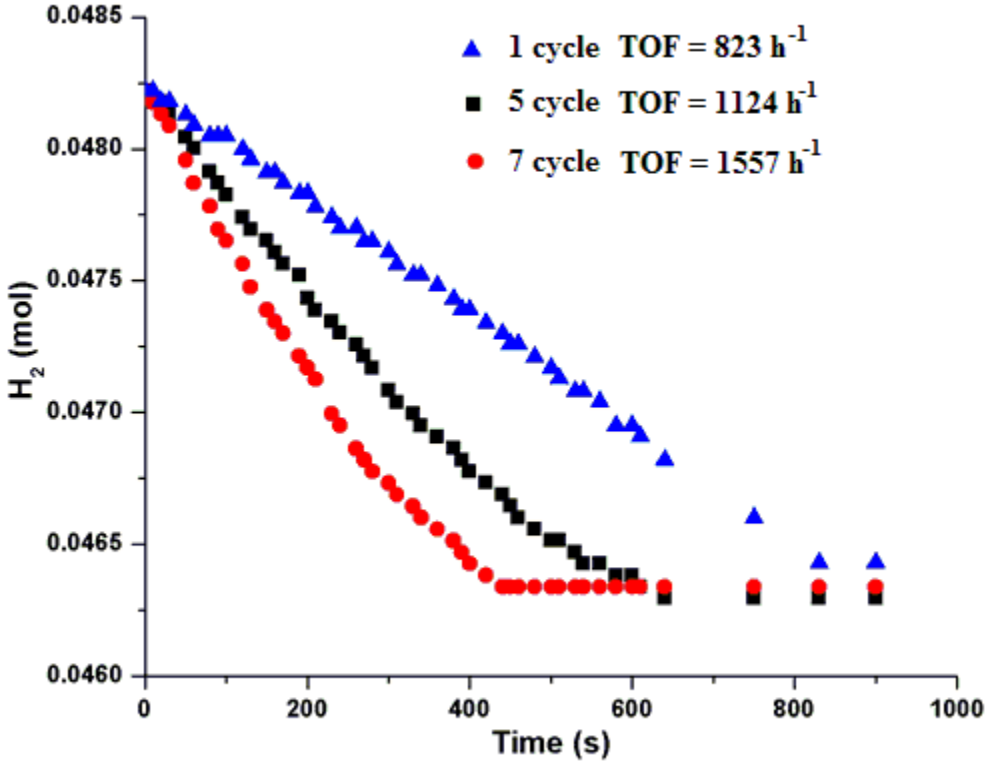

Figure 5. TEM images of the 20:1 Fe@Fe_xO_y/Pd NPs: (A) before hydrogenation reaction; (B) after 4 cycles; and (C) after 6 cycles.

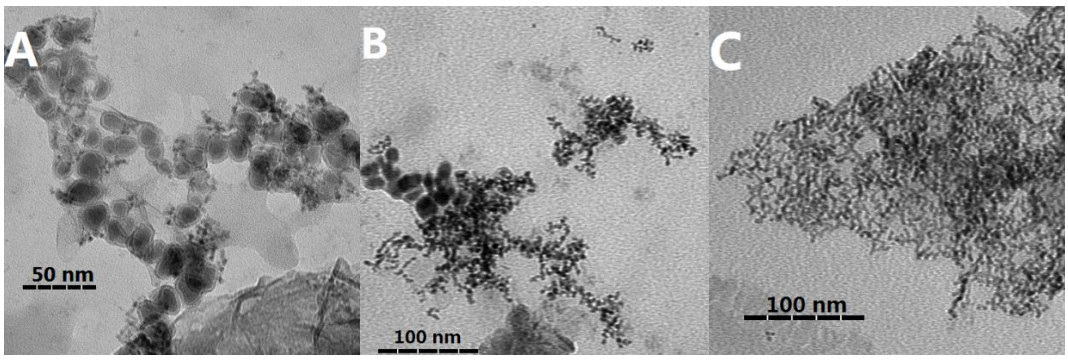

Figure 6. The Pd L-edge (A) and Fe K-edge (B) XANES spectra of the 20:1 molar ratio Fe@Fe_xO_y/Pd NPs.

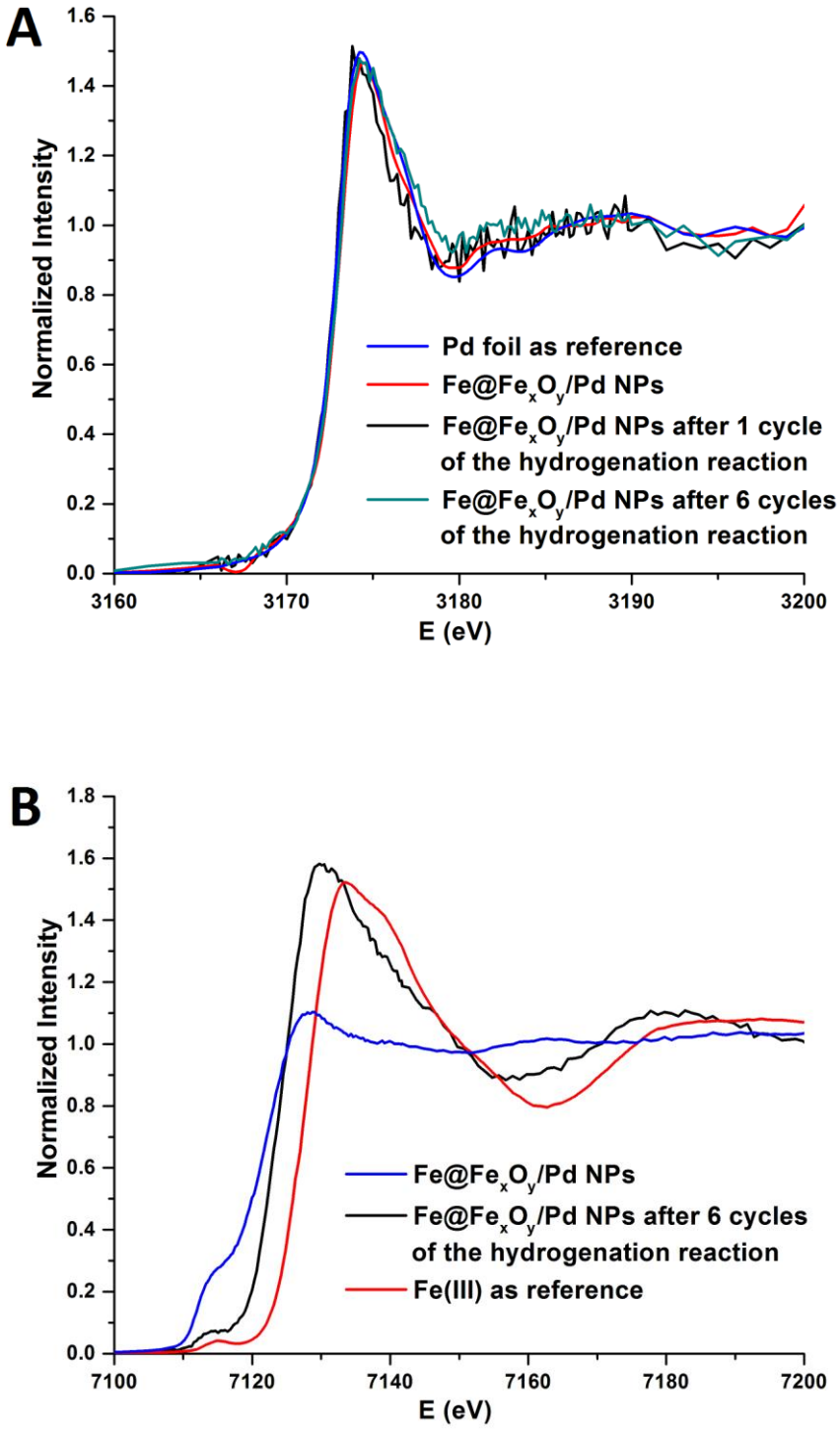

Figure 7. The hydrogenation setup for *in situ* fluorescence XANES studies.

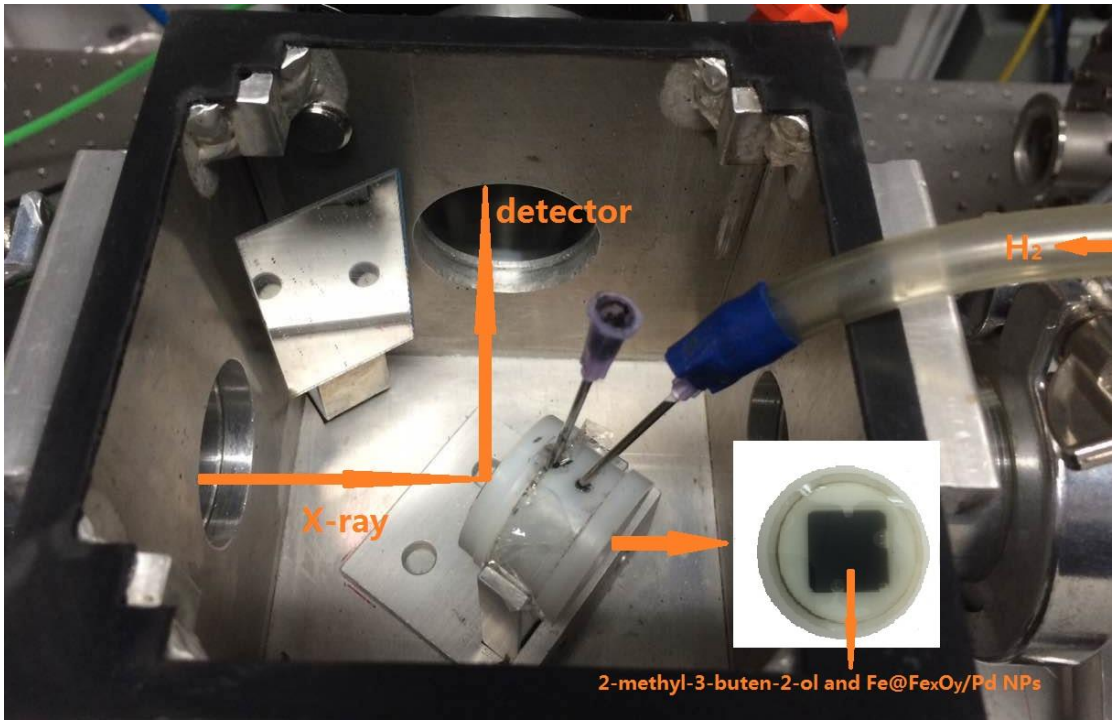

Figure 8. The Pd L-edge (A) and Fe K-edge (B) XANES spectra of the 20:1 molar ratio Fe@Fe_xO_y/Pd NPs in the hydrogenation reaction using water as s solvent.

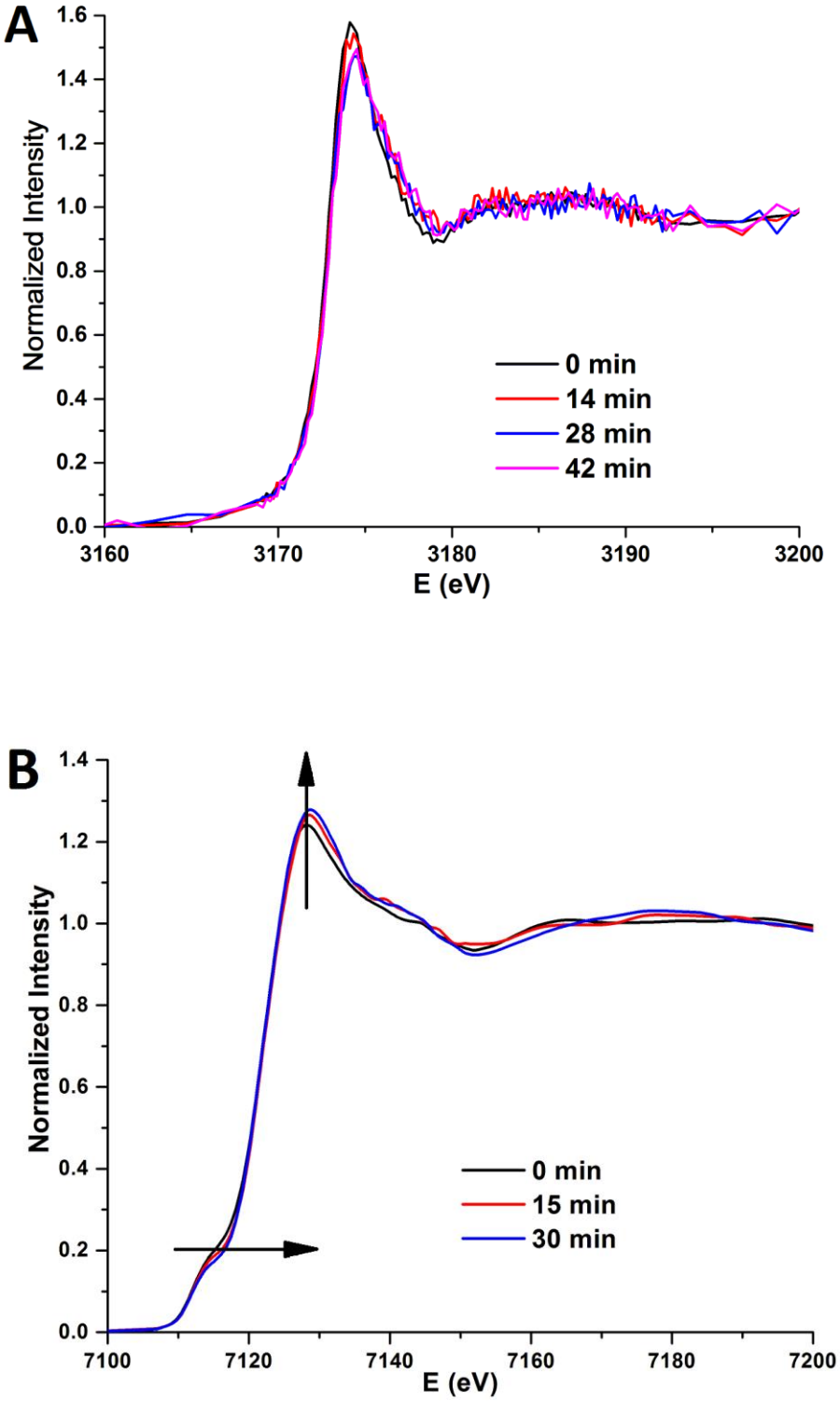

Figure 9. The Fe K-edge XANES spectra of the 20:1 Fe@Fe_xO_y/Pd NPs in the hydrogenation reaction using ethanol as a solvent.

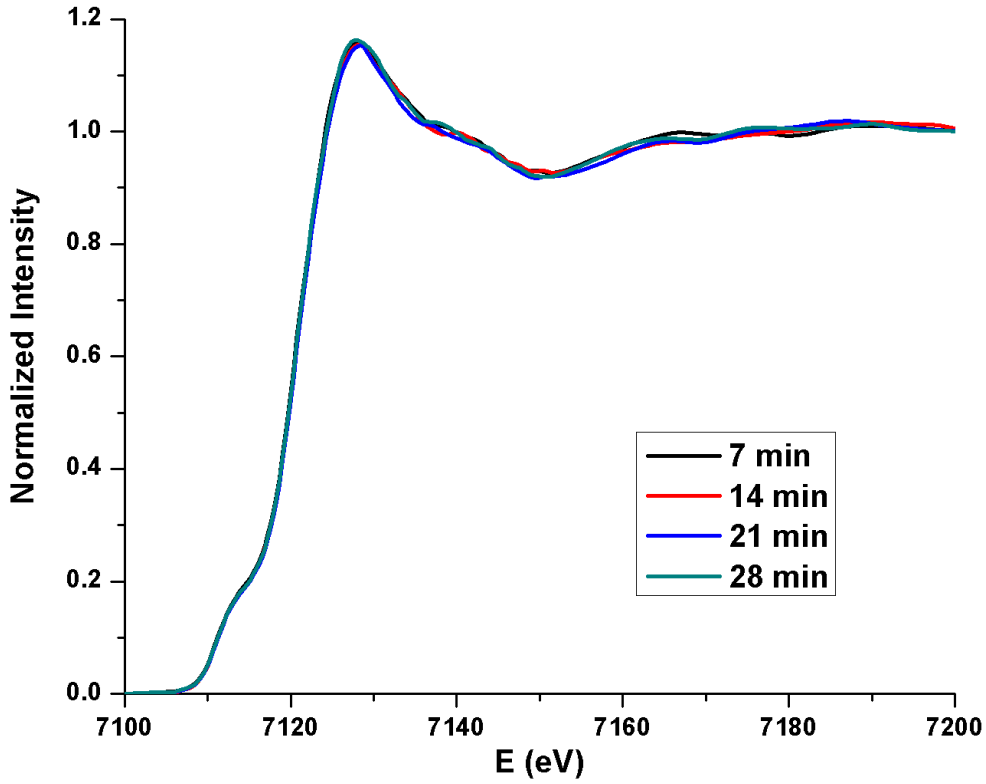

Figure 10. The rates of hydrogen consumption for the hydrogenation of 2-methyl-3-buten-2-ol using the 5:1 $Fe@Fe_xO_y$/Pd NPs as catalysts in either water or ethanol.

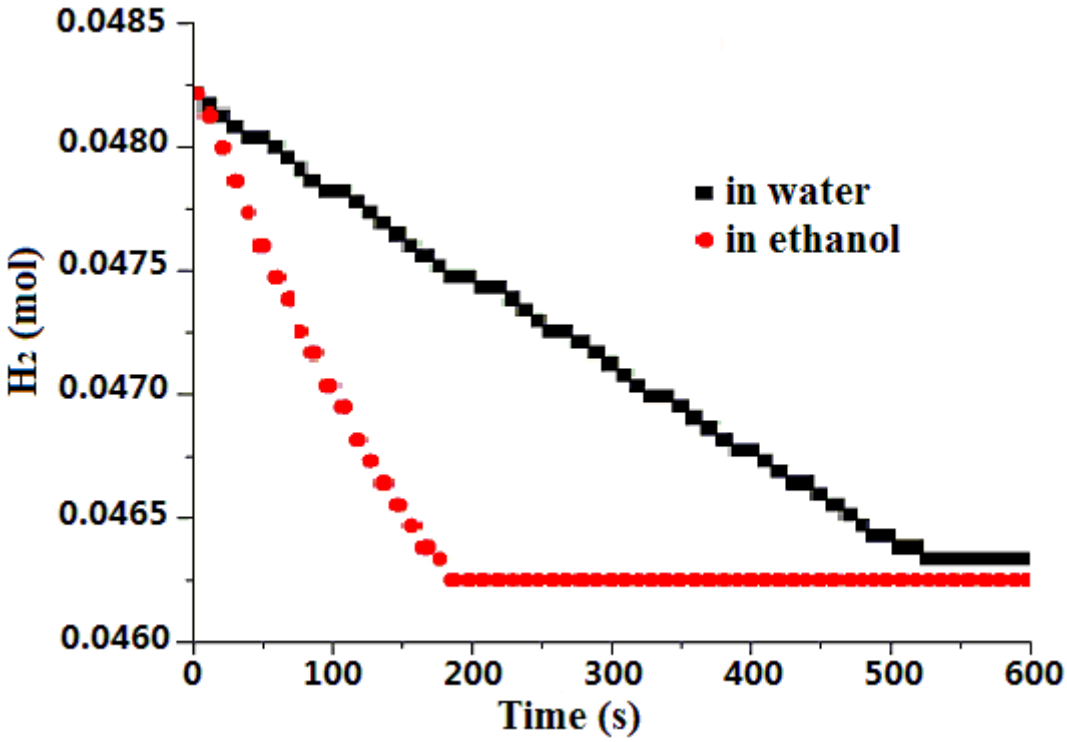

TOC Graphic

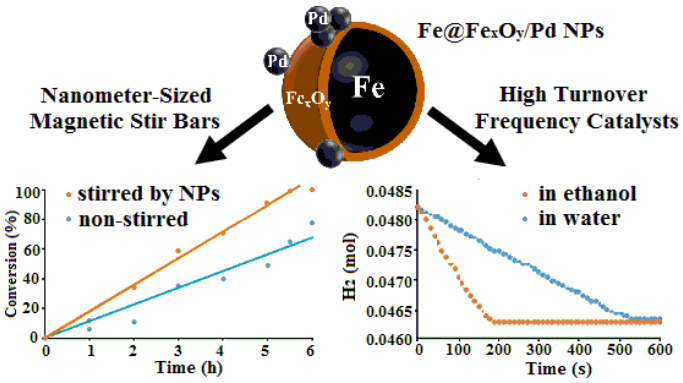
Pd
Pd
Fe
Fe@FexOy/Pd NPs
Nanometer-Sized
Magnetic Stir Bars
High Turnover
Frequency Catalysts
stirred by NPs
non-stirred
Conversion (%)
Time (h)
in ethanol
in water
H2 (mol)
Time (s)